ELSEVIER

#### Contents lists available at ScienceDirect

# NeuroImage

journal homepage: www.elsevier.com/locate/ynimg





# Multiparametric mapping of brain oxygen consumption with resting state calibrated functional MRI

Antonio M. Chiarelli <sup>a,b,\*</sup>, Michael Germuska <sup>c,d</sup>, Davide Di Censo <sup>a,b</sup>, Ian Driver <sup>c</sup>, Maria Eugenia Caligiuri <sup>e</sup>, Hannah Thomas <sup>c</sup>, Svetla Manolova <sup>c</sup>, Hannah L Chandler <sup>c</sup>, Alessandra Caporale <sup>a,b</sup>, Emma Biondetti <sup>a,b</sup>, Richard G. Wise <sup>a,b</sup>

- a University G. D'Annunzio of Chieti-Pescara, Department of Neurosciences, Imaging, and Clinical Sciences, Via Luigi Polacchi 11, Chieti 66100, Italy
- b University G. D'Annunzio of Chieti-Pescara, Institute for Advanced Biomedical Technologies, Via Luigi Polacchi 11, Chieti, 66100, Italy
- <sup>c</sup> Cardiff University Brain Research Imaging Centre (CUBRIC), Cardiff University, School of Physics and Astronomy, Cardiff, United Kingdom
- d Department of Radiology, University of California Davis Medical Center, Sacramento, CA, United States
- e University Magna Graecia of Catanzaro, Department of Medical and Surgical Sciences, Neuroscience Research Center, UMG, Catanzaro, Italy

#### ARTICLE INFO

# Keywords: Resting-state calibrated fMRI Cerebrovascular reactivity (CVR) Maximum BOLD modulation Oxygen extraction fraction (OEF) Cerebral metabolic rate of oxygen (CMRO<sub>2</sub>)

#### ABSTRACT

BOLD and cerebral blood flow (CBF) signal perturbations induced by isometabolic vasodilation enable the estimation of BOLD and CBF cerebrovascular reactivities (CVRs) and calibration of the BOLD signal through inference of its maximum change (M). We developed a BOLD and oxygen-transport modelling approach that uses a hypercapnic estimate of M to map the oxygen extraction fraction (OEF) and cerebral metabolic rate of oxygen (CMRO<sub>2</sub>). Inducing hypercapnia requires  $CO_2$  inhalation or volitional breath-holding (BH). We present a calibrated fMRI framework aiming to overcome the limitations of induced hypercapnia that exploits endogenous resting-state (RS) modulations in brain hemodynamics. This approach was compared against BH. We derived a fitting regressor representing a non-metabolically demanding vascular signal from the average grey matter (GM) BOLD obtaining similar parametric maps between BH and a 10-min RS. Associations between average GM values were M: r=0.70, OEF: r=0.88, CMRO<sub>2</sub>: r=0.94 (p-values<10<sup>-4</sup>) with slight underestimation of parameters derived from RS (r=10%) compared to BH. The most informative frequency range to extract a vascular regressor was in the high-frequency portion of the RS spectrum (oscillation times <20 s), where modulations in systemic pressure induced by breathing occur. RS fMRI estimation of CMRO<sub>2</sub> appears feasible, and it holds promise for research and clinical application.

#### 1. Introduction

The human brain consumes approximately 20% of the energy available to the body, primarily for restoring synaptic ionic gradients and supporting intrinsic or spontaneous activity in communicating neurons at rest (Magistretti and Allaman, 2013). Since the brain does not have significant reserves of its metabolic substrates, i.e., glucose and oxygen, its ability to regulate the local blood supply through cerebral blood flow (CBF) is key to maintaining brain function and tissue integrity (Raz et al., 2007). Cerebrovascular reactivity (CVR) reflects the capacity of the brain's vasculature to increase CBF following a vaso-dilatory stimulus. It is an essential property of the brain's blood vessels

to maintain nutrient supply in the face of changing demand (Carrera et al., 2009; Chiarelli et al., 2022b; Liu et al., 2019). Neural energy consumption is reflected in the cerebral metabolic rate of oxygen consumption (CMRO<sub>2</sub>), given that brain metabolism is mainly oxidative (Zauner et al., 2002). Therefore, both CVR and CMRO<sub>2</sub> may be considered important markers of brain physiology and pathology (Pillai and Mikulis, 2015; Watts et al., 2018).

Magnetic resonance imaging (MRI) can quantify both CVR and CMRO<sub>2</sub>. CVR is assessed through dynamic evaluation of MRI signals that are sensitive to CBF. CMRO<sub>2</sub> is quantified through concurrent measures of baseline CBF and venous oxygen saturation (SvO<sub>2</sub>, or oxygen extraction fraction, OEF) which are combined, using the Fick Principle,

E-mail addresses: antonio.chiarelli@unich.it (A.M. Chiarelli), magermuska@health.ucdavis.edu (M. Germuska), davide.dicenso@unich.it (D. Di Censo), DriverI@cardiff.ac.uk (I. Driver), me.caligiuri@unicz.it (M.E. Caligiuri), ThomasH66@cardiff.ac.uk (H. Thomas), ManolovaS@cardiff.ac.uk (S. Manolova), ChandlerHL1@cardiff.ac.uk (H.L. Chandler), alessandra.caporale@unich.it (A. Caporale), emma.biondetti@unich.it (E. Biondetti), richard.wise@unich.it (R.G. Wise).

https://doi.org/10.1016/j.neuroimage.2025.121465

Received 8 January 2025; Received in revised form 20 August 2025; Accepted 15 September 2025 Available online 18 September 2025

<sup>\*</sup> Corresponding author.

to estimate CMRO<sub>2</sub>. CBF can be efficiently mapped in the grey matter (GM) using Arterial Spin Labelling (ASL), one of several different MRI approaches available. SvO2 and thus OEF can be evaluated using various MRI methods that exploit the paramagnetic properties of deoxyhemoglobin (dHb). Calibrated functional MRI (fMRI) approaches exploit dynamic Blood Oxygen Level Dependent (BOLD) and ASL acquisitions (Bright et al., 2019; Chen et al., 2022; Davis et al., 1998; Hoge, 2012) acquired during isometabolic modulations of brain physiology to derive the maximum BOLD signal change (M), which is the BOLD signal obtainable with the complete removal of dHb from the voxel. In contrast to other MRI approaches that map brain oxygenation, such as those based on relaxometry (e.g., quantitative BOLD, qBOLD) or on phase images (e.g., quantitative susceptibility mapping, QSM) (He et al., 2008; Zhang et al., 2015), calibrated fMRI methods are insensitive to non-blood sources of susceptibility, with dHb being the only paramagnetic substance that changes its concentration over time within the acquisition period. Initial implementations of calibrated fMRI used a single respiratory challenge (primarily a hypercapnic one) to estimate M through the Davis Model of the BOLD signal, which could then be applied in subsequent BOLD-ASL recordings to infer modulations in CMRO<sub>2</sub> and the flow-metabolism coupling during a task (Davis et al., 1998; Hoge, 2012). Notably, gas-free calibrated fMRI attempted to estimate M from quantitative R2' relaxometry measures (Chen et al., 2022; Kida et al., 2000), facing the same limitations as the more recent qBOLD approach. Due to the dependence of M on both baseline OEF and venous blood volume (CBV<sub>v</sub>), quantification of baseline CMRO<sub>2</sub> was not possible using these methods. The method introduced for the quantitative mapping of CMRO2 through fMRI relies on a dual calibration approach (dc-fMRI), in which cerebral hemoglobin saturation is modulated with two separate respiratory challenges (one hypercapnic and one hyperoxic) (Bulte et al., 2012; Gauthier et al., 2012; Gauthier and Hoge, 2012; Germuska and Wise, 2019) to decouple the contributions of baseline CBV<sub>v</sub> and OEF to M. Although dc-fMRI has been applied in clinical research studies (Chandler et al., 2023), its adoption is limited by the low signal-to-noise ratio (SNR) intrinsic to this technique and by the complex apparatus and gas-challenge paradigm required to induce hypercapnia and hyperoxia (Germuska and Wise, 2019).

We recently developed a calibrated fMRI approach that integrates the Davis Model of BOLD signal (Davis et al., 1998) with a biophysical model of oxygen diffusion from capillaries to mitochondria, requiring only one hypercapnia-based measure of M to estimate resting CMRO2 (Chiarelli et al., 2022a; Driver et al., 2024; Hayashi et al., 2003; Hyder et al., 1998). This simple diffusion model assumes that steady-state oxygen extraction depends on the product of the mean blood transit time in capillaries and the oxygen pressure gradient between capillaries and the mitochondria at the end of the diffusion path. Using this model and assuming low oxygen pressure at the mitochondria (PmO2), the model describes the baseline CBV<sub>v</sub> as a function of baseline CBF (that we measure with ASL) and OEF (Gjedde, 2002; Gjedde et al., 1999). Modelling studies and experimental comparison with the dual-calibrated approach demonstrated the viability of this method, at least within plausible ranges of physiological parameters and in healthy subjects (Chiarelli et al., 2022a). However, this approach still requires a hypercapnic gas challenge or an alternative hypercapnic stimulus such as breath-holding (BH), limiting its applicability in some settings (e.g. in sedated or uncompliant individuals or participants with altered lung function) (Driver et al., 2024).

It would be preferable in many instances to estimate M directly from resting-state (RS) data, without the need for an explicit hypercapnic stimulus. However, the estimation of M requires the measurement of isometabolic fluctuations in the BOLD and ASL signal, whereas the local RS modulations are known to have a non-isometabolic component (Fukunaga et al., 2008). Nonetheless, isometabolic vascular fluctuations are present during RS (Biswal et al., 2007; Chang and Glover, 2009; Kannurpatti et al., 2011; Kannurpatti and Biswal, 2008; Tak et al., 2015). An isometabolic signal might be extracted by exploiting natural

variation in the cerebral blood vessel tone or systemic pressure, induced by respiration or other endogenous physiological factors (Birn et al., 2008; Chang and Glover, 2009). The signal, which we posit is unrelated to local brain metabolism, could then be used as a regressor to estimate maps of BOLD and CBF signal changes relative to this signal (depicting the local vascular response following the global endogenous stimulus, i. e., relative CVRBOLD and CVRCBF) and infer M. These approaches have previously been attempted on BOLD signal recordings to estimate CVR<sub>BOLD</sub>. For example, the significant temporal association between end-tidal partial pressure of CO2 (PETCO2, a marker of CO2 concentration in arteries, CaCO2) and the BOLD signal at rest suggests the possibility to use such a signal to infer CVR<sub>BOLD</sub> (Chang and Glover, 2009; Golestani et al., 2016; Wise et al., 2004). However, using the PETCO2 signal requires the expired air to be sampled from a mask or a nasal cannula, and practically, in our experience, the acquired signals may be contaminated by imperfect sampling and by small variations in the expiration pattern. Although mostly inconsequential when large modulations in P<sub>ET</sub>CO<sub>2</sub> occur, for example, during a hypercapnic stimulus, these effects may be significant when trying to reliably estimate the small temporal fluctuations of the signal of interest during rest. An alternative approach was proposed by Liu and Colleagues (Liu et al., 2017), which suggested using the global BOLD signal modulation as representative of a purely vascular, non-metabolically demanding, signal. Global, non-region-specific fluctuations in BOLD MRI signal are known to be related to several physiological mechanisms, including cardiac cycle, breathing cycle and slow physiological variations in blood pressure (Liu et al., 2017; Murphy et al., 2013; Wise et al., 2004). This approach is consistent, for example, with the procedures frequently adopted when conducting RS analysis of brain activity, where the global signal is generally considered of vascular origin and is regressed out from each voxel as a pre-processing step (Macey et al., 2004; Murphy et al., 2009; Rogers et al., 2007). The approach implemented by Liu and colleagues was demonstrated to be reproducible and accurate compared to the CO2 inhalation method.

Here, we propose to extend such an approach to concurrent RS BOLD-ASL recordings and combine this experimental method with our recently proposed modelling of the BOLD signal. This work aims to deliver a novel stimulation-free RS calibrated fMRI framework that enables calculation of maps of relative  $\text{CVR}_{\text{BOLD}}$  and  $\text{CVR}_{\text{CBF}}$  and, by combining these two, maps of the maximum BOLD modulation M. M can then be used to derive relevant quantitative information on OEF and  $\text{CMRO}_2$ . The approach is validated against calibrated fMRI relying on a hypercapnic stimulus, namely, breath-holding (BH) (Driver et al., 2024; Thomason et al., 2006).

# 2. Methods

#### 2.1. BOLD analytical modeling

Here, we summarize the biophysical model used for parameter estimation. For a detailed description of the model please refer to Chiarelli & Germuska (Chiarelli et al., 2022a) and the associated Supplementary Material.

#### 2.1.1. Measuring the maximum BOLD signal

For small perturbations of  $R_2^{\star}$  induced by changes in dHb, the steady-state fractional BOLD signal can be expressed as (Buxton, 2009; Germuska and Wise, 2019):

$$\frac{\Delta BOLD}{BOLD} = M \cdot \left\{ 1 - \left( \frac{CBV_{\nu,m}}{CBV_{\nu}} \right) \cdot \left( \frac{1 - S_{\nu}O_{2,m}}{1 - S_{\nu}O_{2}} \right)^{\beta} \right\}$$
(1)

where  $CBV_v$  is the BOLD-sensitive blood volume (which actually refers to the blood volume where dHb is confined, which is primarily of venous origin but it also has a smaller contribution from capillaries),  $S_vO_2$  is the venous saturation, and the subscript m depicts a temporal modulation.

The constant parameters are M, which is the maximum BOLD modulation (a function of baseline dHb), and  $\beta$ , which is a field strength and vessel geometry dependent constant larger than 1 describing the supralinear effect of dHb in blood on the BOLD signal ( $\beta$  =1.3 at 3T) (Bulte et al., 2012). Using the Grubb relation (Grubb et al., 1974) and the Fick Principle (refer to Eq. 5), Eq. 1 can be expressed as a function of modulation in CBF and CMRO<sub>2</sub> as:

$$\frac{\Delta BOLD}{BOLD} = M \cdot \left\{ 1 - \left( \frac{CBF_m}{CBF} \right)^{\alpha - \beta} \cdot \left( \frac{CMRO_{2,m}}{CMRO_2} \right)^{\beta} \right\}$$
 (2)

where  $\alpha$  is the Grubb exponent ( $\alpha\!=\!0.38$ ). Assuming isometabolism with hypercapnia, M can be measured through fractional BOLD and CBF changes as:

$$M = \frac{\frac{\Delta BOLD}{BOLD}}{\left\{1 - \left(1 + \frac{\Delta CBF}{CBF}\right)^{\alpha - \beta}\right\}} = \frac{CVR_{BOLD} \cdot \Delta \nu as}{\left\{1 - \left(1 + CVR_{CBF} \cdot \Delta \nu as\right)^{\alpha - \beta}\right\}}$$
(3)

where BOLD and CBF fractional changes can be divided by a measure of the vasoactive stimulus amplitude ( $\Delta vas$ , often measured in units of mmHg of  $P_{ET}CO_2$  change following hypercapnia) to infer  $CVR_{BOLD}$  (e.g., in units of %BOLD/mmHg) and  $CVR_{CBF}$  (e.g., in units of % CBF/mmHg).

Although in this work Eq. 3 was used for the computation of M, it is worth noting that Eq. 3 can be linearized relative to the modulation in CBF, assuming it to be small, to obtain:

$$M = \frac{\frac{\Delta BOLD}{BOLD}}{(\beta - \alpha) \cdot \left(\frac{\Delta CBF}{CBF}\right)} = \frac{CVR_{BOLD}}{(\beta - \alpha) \cdot CVR_{CBF}}$$
(4)

Since  $\beta - \alpha \approx 1$ , M is almost equal to the ratio of the fractional changes of BOLD and CBF (or CVR<sub>BOLD</sub>/ CVR<sub>CBF</sub>).

#### 2.1.2. Measuring CMRO<sub>2</sub>

Baseline CMRO<sub>2</sub> can be estimated with MRI through the Fick Principle (the conservation of oxygen mass):

$$CMRO_2 = CBF \cdot OEF \cdot CaO_2 \tag{5}$$

Baseline CBF can be inferred from the baseline ASL signal, whereas  $CaO_2$  can be estimated from end-tidal partial pressure of  $O_2$  ( $P_{ET}O_2$ ) measurements (refer to Eqs 14 and 15). OEF is defined as:

$$OEF = \frac{CaO_2 - CvO_2}{CaO_2} \tag{6}$$

with  $CaO_2$  and  $CvO_2$  being arterial and venous blood oxygen content, respectively. The maximum BOLD signal M is expressed as a function of resting  $CBV_v$  and  $SvO_2$  (or OEF) as (Buxton, 2009; Germuska and Wise, 2019):

$$M = TE \cdot A \cdot CBV_{v} \cdot ((1 - S_{v}O_{2}) \cdot [Hb])^{\beta}$$

$$= TE \cdot A \cdot CBV_{v} \cdot \left( \left( 1 - \frac{CaO_{2}}{\varphi \cdot [Hb]} \cdot (1 - OEF) \right) \cdot [Hb] \right)^{\beta}$$
(7)

where TE is the echo time of the acquisition, A is a field strength and vessel geometry dependent constant,  $\phi$  is the oxygen binding capacity of hemoglobin ( $\phi{=}1.34$  mL/g) and [Hb] is the concentration of hemoglobin in blood. Of note, the link between  $SvO_2$  and OEF is derived assuming negligible plasma  $O_2$  content on the venous side. (Chiarelli et al., 2022a). TE is known, A can be assumed or derived through modelling, and [Hb] can be measured using blood samples or by measuring the T1 of blood in a large vessel, which primarily depends on [Hb].

Eq. 7 has two physiological unknowns, baseline  $\mathsf{CBV}_v$  and  $\mathsf{OEF}$ , which makes it impossible to solve for  $\mathsf{OEF}$  through a single estimate of M without additional constraints.

We recently introduced into the calibrated fMRI framework a simple

model of diffusion of oxygen from capillaries to mitochondria that states that the steady-state extraction of oxygen from capillaries is proportional to the product of mean capillary transit time (MCTT) and the pressure gradient along the diffusion path:

$$OEF \cdot CaO_2 = k \cdot MCTT \cdot \left( P_{50} \cdot \sqrt[h]{\frac{2}{OEF} - 1} - P_m O_2 \right)$$
(8)

where k is the effective permeability of the capillary and the surrounding brain tissue,  $\left(P_{50}\cdot \sqrt[h]{\frac{2}{OEF}-1}\right)$  is the capillary oxygen pressure,

and  $PmO_2$  is the oxygen pressure at the mitochondria. Capillary oxygen pressure depends on OEF,  $P_{50}$ , which is the oxygen partial pressure when half of Hb is saturated (generally  $P_{50}{\approx}26$  mmHg;  $P_{50}$  can be inferred from a measure of  $P_aCO_2$ ), and h, which is the Hill constant (h=2.8). Eq. 8 can be rewritten via the central volume principle (i.e., MCTT=CBV<sub>cap</sub>/CBF) with CBV of capillaries (CBV<sub>cap</sub>) being a fraction of CBV<sub>v</sub> (i.e., CBV<sub>v</sub>= $P_0$ -CBV<sub>cap</sub>) as:

$$CBF \cdot OEF \cdot CaO_2 = \frac{k}{\rho} \cdot CBV_{\nu} \cdot \left( P_{50} \cdot \sqrt[h]{\frac{2}{OEF_0} - 1} - P_m O_2 \right)$$
(9)

Eq. 9 allows us to express CBV<sub>v</sub> as a function of CBF and OEF as:

$$CBV_{\nu} = CBF \frac{\rho}{k} \cdot \frac{OEF \cdot CaO_2}{\left(P_{50} \cdot \sqrt[h]{\frac{2}{OEF} - 1} - P_m O_2\right)}$$
(10)

where the CBF is multiplied by  $\frac{\rho}{k}$ .  $\underbrace{\left(P_{50}\cdot\sqrt[h]{\frac{2}{OEF}-1}-P_{m}O_{2}\right)}_{}$  which is the MTT

within the venous compartment.

Eq. 10 can be integrated into Eq. 7 to obtain:

$$M = TE \cdot \frac{A \cdot \rho}{k} \cdot \frac{CBF \cdot OEF \cdot CaO_2 \cdot \left(\left(1 - \frac{CaO_2}{\varphi[Hb]} \cdot (1 - OEF)\right) \cdot [Hb]\right)^{\beta}}{\left(P_{50} \cdot \sqrt[h]{\frac{2}{OEF} - 1} - P_mO_2\right)}$$
(11)

TE,  $\beta$  and h in Eq. 11 are known constants related to the MRI acquisition scheme, MRI physics and oxygen bounding properties of hemoglobin, whereas quantitative CBF at rest can be measured with ASL (refer to the Data Analysis, fMRI Processing paragraph). Moreover baseline values of  $P_{50}$ , CaO<sub>2</sub> and [Hb] can be estimated from  $P_{ET}CO_2$  and  $P_{ET}O_2$  traces and from measures of blood hematocrit (please refer to the Methods Section, paragraphs Data Analysis, Analysis of Gas Recordings and Estimation of Blood Hemoglobin Concentration). Since the lumped parameter  $\frac{A\cdot p}{k}$  should be near constant in the absence of significant vascular remodelling and PmO<sub>2</sub> is generally small in the human brain (PmO<sub>2</sub>≈0) (Gjedde, 2002), Eq. 11 can be used to infer OEF from measures of M and hence CMRO<sub>2</sub> through Eq. 5. We assigned a value of 8.8 s<sup>-1</sup>g<sup>-\beta</sup>dL<sup>\beta</sup>/(\mumol/mmHg/mL/min) to the term  $\frac{A\cdot p}{k}$ , matching our previously established in-vivo measurement when PmO<sub>2</sub> is fixed to 0 mmHg (Chiarelli et al., 2022a).

# 2.2. Data acquisition

Thirty-three healthy volunteers (16 females, age (mean  $\pm$  standard deviation) = 24.5  $\pm$  6.0 years) were recruited at CUBRIC, Cardiff University, Cardiff, UK. The study was performed in accordance with the Declaration of Helsinki and was approved by the Cardiff University, School of Psychology Ethics Committee. Written consent was obtained from each participant. Data were acquired using a Siemens MAGNETOM Prisma (Siemens Healthcare GmbH, Erlangen, Germany) 3 T clinical scanner with a 32-channel receiver head coil (Siemens Healthcare GmbH, Erlangen, Germany).

BOLD-ASL fMRI data were acquired during RS and BH using an inhouse PCASL acquisition scheme with pre-saturation and background suppression (Okell et al., 2013) and a dual-excitation (DEXI) echo planar imaging (EPI) 2D readout (Schmithorst et al., 2014). The labelling duration (t) and the Post Label Delay (PLD) were both set to 1.5 s, GRAPPA acceleration (factor = 3) was used with  $TE_1 = 10$  ms and  $TE_2 =$ 30 ms. An effective TR of 4.4 s was used to acquire 15 slices, with an in-plane resolution of  $3.4 \times 3.4 \text{ mm}^2$  and a slice thickness of 6 mm with a 20% slice gap. The RS protocol consisted of a 10-minute and 16-second DEXI PCASL acquisition. During RS the participants were instructed to fix their vision on a cross at the center of the screen with a grey background. The BH protocol was visually guided via instructions projected onto the same screen and included 10 repeats of a 20 second duration post-expiratory breath-holding with 30 seconds of recovery (normal breathing) in between. Subjects were instructed to fully breathe out at the end of each BH to enable estimation of arterial content of  ${\rm O}_2$  and CO2. During the fMRI recordings, CO2 and O2 in the expired air were evaluated from the volunteer's nasal cannula using a gas analyzer (AEI Technologies, Pittsburgh, PA, USA).

Calibration images (S<sub>0</sub>) were acquired for ASL quantification with PCASL labelling and background suppression pulses switched off, with TR=6 s, and TE=10 ms (Germuska et al., 2019). Two S<sub>0</sub> images were acquired with opposite phase encoding directions twice, before RS and BH, to allow for distortion corrections in the BOLD-ASL fMRI acquisition. An in-house inversion recovery sequence, with a single slice readout, was acquired with the imaging plane intersecting the superior sagittal sinus in order to estimate the longitudinal relaxation time constant (T1) of blood and infer [Hb] (Varela et al., 2011). The sequence consisted of a nonselective inversion pulse followed by fast (TR/TE=150/22ms) acquisitions of a single slice (EPI readout, 3-mm slice thickness, 128×128 matrix, 1.8×1.8 mm<sup>2</sup> in-plane resolution) acquired for 6 seconds. The short TR saturated the static tissue and highlighted the longitudinal magnetization recovery of the inflowing blood. 16 inversions were performed to increase the confidence in the T1 estimate.

A magnetization-prepared rapid acquisition with gradient echo (MPRAGE) T1-weighted scan was acquired for registration and brain segmentation purposes (matrix  $165\times203\times197$ , 1-mm isotropic resolution, TR/TE = 2100/3.24 ms).

# 2.3. Data analysis

#### 2.3.1. Analysis of gas recordings

 $P_{ET}CO_2$  and  $P_{ET}O_2$  were extracted from  $CO_2$  and  $O_2$  recordings using in-house software developed in Matlab (The MathWorks, Inc. MATLAB R2022b) (Chiarelli et al., 2022a). Average  $P_{ET}CO_2$ , assumed to be in equilibrium with PaCO<sub>2</sub> during RS, was used to infer  $P_{50}$  from estimates of resting blood pH based on the Henderson-Hasselbalch Equation, assuming  $[HCO_3^-]=24$  mmol/L (Gai et al., 2003):

$$pH = 6.1 + \log\left(\frac{[HCO_3^-]}{0.03 \cdot PaCO_2}\right)$$
 (12)

and calculating  $P_{50}$  according to the linear relation (Germuska et al., 2019):

$$P_{50} = 221.87 - 26.37 \cdot pH \tag{13}$$

 $\text{CaO}_2$  was calculated from average  $P_{\text{ET}}O_2$ , assumed equal to  $\text{PaO}_2$  during RS, using the Hill Equation:

$$SaO_2 = \frac{1}{1 + \left(\frac{P_{50}}{PaO_2}\right)^h} \tag{14}$$

and the equation:

$$CaO_2 = \varphi \cdot [Hb] \cdot SaO_2 + \varepsilon \cdot PaO_2 \tag{15}$$

where  $\epsilon$  is the oxygen plasma solubility in blood ( $\epsilon$ =0.0031 mL/mmHg/dL), and [Hb] was estimated through Eq. 16.

#### 2.3.2. Estimation of blood hemoglobin concentration

The T1 of venous blood was estimated from non-linear least squares fitting to a mono-exponential signal model using the long TR approximation,  $S=|a+b\cdot e^{(-TI/T_1)}|$  where TI is the time of inversion. To reduce possible contamination from blood water of non-venous origin, only the first 4 seconds from the inversion were used. Automatic voxel selection for the sagittal sinus was performed by first defining a small rectangular region of interest (ROI) measuring  $60\times30$  mm² around the superior sagittal sinus. Secondly, voxels with intensity above the 50th percentile within this ROI were retained in the third acquired slice, where complete saturation of static tissue was achieved. The blood hematocrit (Hct) was determined from the linear relationship with venous T1 previously reported at 3 T (Lu et al., 2004):

$$T1(s) = \frac{1}{0.83 \cdot Hct + 0.28} \tag{16}$$

Hct was converted to [Hb], assuming a ratio Hct/[Hb]=3 (%dL/g) (Insiripong et al., 2013).

#### 2.3.3. fMRI processing

Both RS and BH fMRI data were processed using FSL (Jenkinson et al., 2012), ANTs (Avants et al., 2011), and in-house Matlab algorithms. Time courses were divided by TE and PCASL tagging (tag/control). Tag and control images for both echoes were motion-corrected with FSL's MCFLIRT (Jenkinson et al., 2002). Initial volumes of tag and control images were rigidly registered using FLIRT to minimize misregistration from tag-control contrast differences. BH and RS volumes were rigidly aligned using ANTs to the brain-extracted  $S_0$  (estimated with FSL BET), acquired with the same phase encoding as the functional scans. Susceptibility distortions were corrected using FSL TOPUP with two  $S_0$  images of different phase encoding direction (Smith et al., 2004). Finally, BH images were registered to RS images using ANTs.

All subsequent analysis was performed in Matlab (The MathWorks, Inc. MATLAB R2022b).

 $TE_1$  surround subtractions ( $\Delta S$ ) were converted into CBF (expressed in quantitative units of mL/100g/min) through the single compartment kinetic model for PCASL with voxelwise  $S_0$  normalization (Alsop et al., 2015):

$$CBF = \frac{6000 \cdot \lambda \cdot e^{\frac{PLD}{T1_b}}}{2 \cdot \eta \cdot \eta_{inv} \cdot T1_b \cdot \left(1 - e^{-\frac{\tau}{T1_b}}\right)} \cdot \left(\frac{\Delta S}{S_0}\right)$$
(17)

where  $\lambda$  is the water partition coefficient ( $\lambda$ = 0.9 mL/g), T1<sub>b</sub> is the T1 relaxation constant of arterial blood (estimated through the inversion recovery acquisition with correction for being arterial blood) (Lu et al., 2004),  $\eta$  is the tagging inversion efficiency ( $\eta$  =0.85), and  $\eta_{inv}$  is a scaling factor to account for the reduction in tagging efficiency due to background suppression (η<sub>inv</sub>=0.88) (Aslan et al., 2010; Mutsaerts et al., 2014). To avoid the confounding effects of spatial high-frequency features of So during normalization, a low-pass filtered version of So was used, estimated through second-order polynomial fitting of the brain-masked S<sub>0</sub>. In order to avoid possible misregistration effects between functional scans and structural images, the time averaged CBF map was used to extract an apparent GM mask. Owing to the much higher perfusion of GM compared to white matter (WM), the presence of GM was evaluated by normalizing the CBF map between its 5<sup>th</sup> and its 95<sup>th</sup> percentile and by setting to zero all values below 0 and above 1 after normalization (to exclude outliers). Voxels were labelled as GM if their normalized value was above 0.5. TE2 volumes were used for BOLD signal

extraction

For the BH task, BOLD and CBF signals were band-pass filtered (Butterworth digital filter, order 4) with cut-off times of  $10 \, \mathrm{s}$  (0.1 Hz of low-pass cut-off frequency) and  $200 \, \mathrm{s}$  (0.005 Hz of high pass cut-off frequency). The low-pass cut-off time of  $10 \, \mathrm{s}$  (0.1 Hz) was chosen to approximate a surrounding averaging required to eliminate any residual perfusion effect on BOLD signal induced by the alternating tagging (considering a Nyquist time of  $8.8 \, \mathrm{s}$ ,  $0.11 \, \mathrm{Hz}$  of Nyquist frequency). The high-pass cut-off time was chosen to eliminate slow drifts without distorting the response and recovery signal to the BH task.

The RS BOLD and CBF signals were band-pass filtered (Butterworth digital filter, order 4) with variable combinations of low-pass and highpass frequency to explore the optimal frequency band to be used. The low-pass cut-off times varied from 10 s (0.1 Hz) to 100 s (0.01 Hz), whereas the high-pass cut-off times varied from 40 s (0.025 Hz) to 300 s (0.003 Hz), please refer to the Results Section, paragraph Effect of Filtering and Recording Time on Resting-State Analysis. The optimal band-pass filter was identified with cut-off times between 10 s and 150 s, which were used for the main results presented.

The following analysis was conducted for both BH and RS. Global GM BOLD signals were calculated as the median value within the GM mask for each time point, following band-pass filtering. These signals were converted to z-scores to represent a vascular signal with zero mean and unit variance. Voxel-wise BOLD and CBF signal modulations relative to the vascular signal were assessed using linear regression within a general linear model (GLM) framework (Friston, 1994). The voxel-wise signal could shift by one sample ( $\pm$  4.4 s) to best correlate with the vascular signal, estimating the local cerebrovascular response time lag relative to the global signal. The regression weight estimated the BOLD or CBF modulation associated with the global vascular signal, expressed as %BOLD and %CBF changes due to the unitary variance of the vascular signal. The Signal-to-Noise Ratio (SNR) of the modulation estimate was calculated by dividing the GLM  $\beta$ -weight by its confidence interval. CVR<sub>BOLD</sub> and CVR<sub>CBF</sub> maps were used to estimate M from Eq. 3. OEF was inferred using Eq. 11, with non-linear inversion through parameter space exploration. CMRO2 was estimated via Eq. 5. Average GM values of the parameters were extracted, and parametric maps were warped onto MNI152 space (using FSL's FNIRT) for average map evaluation across subjects. RS acquisition time effects were investigated by repeating the RS analysis at intervals from 20 s, increasing in 20 s steps, up to the entire available acquisition time.

#### 2.4. Statistical analysis

Pearson's correlations and t-tests were performed to assess pairwise associations and biases between the parameters estimated through BH and RS. Normality evaluation was performed prior to statistical inference using the Kolmogorov-Smirnov test. A null hypothesis probability below 5% (p<0.05) was considered statistically significant.

## 3. Results

#### 3.1. Arterial oxygenation

 $P_{ET}O_2$  during the RS recordings was, on average,  $P_{ET}O_2{=}111{\pm}7$  mmHg (mean $\pm$ std), whereas the average  $P_{ET}CO_2$  was  $P_{ET}CO_2{=}36{\pm}3$  mmHg.  $P_{ET}O_2$  and  $P_{ET}CO_2$  were respectively assumed to be in equilibrium with PaO $_2$  and PaCO $_2$ . From Eqs 12 and 13, the PaCO $_2$  delivered an estimated average  $P_{50}{=}25.6{\pm}1.4$  mmHg. From Eq. 14, an average SaO $_2{=}98.3{\pm}0.5$ % was estimated. The  $T_1$  of blood, inferred from the inversion recovery acquisition, was on average  $T_{1,blood}{=}1632{\pm}117$  ms, which delivered, through Eq. 16, a hematocrit of Hct=40.5 ${\pm}5.1$ % and a hemoglobin concentration in blood of [Hb]=13.5 ${\pm}1.7$  g/dL. From Eq. 15, the average blood oxygen content was CaO $_2{=}17.9{\pm}2.2$  mL/dL.

#### 3.2. Vascular signal and cerebrovascular reactivity

Fig. 1a reports an example, for a representative subject, of the time-averaged RS CBF map and the corresponding apparent GM mask. Fig. 1b depicts, for the same subject, the average GM BOLD signal extracted for the BH and the RS recordings. Clear periodic modulations of a few percentage points of the BOLD signal are visible for the BH. These modulations are induced by changes in flow caused by the hypercapnic BH task. The RS modulation exhibits, as expected, aperiodic and smaller fluctuations. These signals were normalized (converted to z-scores) and assumed to represent an isometabolic vascular signal to estimate relative  $\text{CVR}_{\text{BOLD}}$  and  $\text{CVR}_{\text{CBF}}$ .

Fig. 2a reports boxplots showing the variability (standard deviation after bandpass filtering) of the voxel-wise and global BOLD (upper row, left image) and CBF (upper row, right image) signals in the gray matter (GM) during BH and RS. Additionally, Fig. 2a presents the estimated average GM CVR<sub>BOLD</sub> and CVR<sub>CBF</sub> (lower row) for both BH and RS. The voxel-wise BOLD variability in the GM was  $1.3\pm0.8$  % during BH and 1.2 $\pm 0.7$  % during RS, while the global GM BOLD signal variability was 0.7  $\pm 0.1$  % during BH and  $0.5\pm 0.3$  % during RS. The voxel-wise CBF variability in the GM was  $59\pm17$  % during BH and  $58\pm27$  % during RS, whereas the global GM CBF signal variability was 35±12 % during BH and 25 $\pm$ 20 % during RS. The CVR<sub>BOLD</sub> in the GM was 0.74 $\pm$ 0.17 % for BH and  $0.40\pm0.18$  % for RS. The CVR<sub>CBF</sub> in the GM was  $11.9\pm5.1$  % for BH and  $7.2\pm2.6$  % for RS. The CVR metrics obtained represent the variability in the voxel-wise signal (% of signal change) that was explained by the normalized (z-scored) global GM BOLD signal (after allowing for  $\pm 1$  TR,  $\pm 4.4$  seconds time lag). Since the global regressor is the same for both BOLD and CBF, their values are comparable within each subject and condition. It is important to note that, although CVR<sub>BOLD</sub> and CVR<sub>CBF</sub> are larger for BH compared to RS, the ratio between the two is similar. The ratio of the two CVRs (apart from mild nonlinearities and scaling parameters) is close to M (as shown in Eqs 3 and 4). Figs 2b and 2c present images of CVR<sub>BOLD</sub> and CVR<sub>CBF</sub> (the images were z-scored to highlight spatial similarities), and cerebrovascular response time lag for an exemple subject (upper rows for each subplot) as well as average maps in MNI space (lower rows for each subplot). The maps depicted were derived from BH (left column for each subplot) or RS (right column for each subplot). Spatial similarities between the BH and RS-derived maps are evident upon visual inspection. Comparing average maps between BH and RS, CVRBOLD exhibited a spatial correlation of r=0.74, whereas CVR<sub>CBF</sub> had a spatial correlation of r=0.23 (all p's< 10<sup>-4</sup>). The spatial correlations of cerebrovascular response latency were r=0.65 for BOLD and r=0.23 for CBF (all p's $<10^{-4}$ ). The average GM SNRs with BH were 15.6 $\pm$ 3.5 and 4.9 $\pm$ 1.4 for CVR<sub>BOLD</sub> and CVR<sub>CBF</sub>, respectively. The average GM SNR with RS were  $8.9\pm3.1$  and  $3.5.0\pm1.4$ for CVR<sub>BOLD</sub> and CVR<sub>CBF</sub>, respectively.

# 3.3. Maximum BOLD modulation and brain oxygen consumption

Fig. 3 displays images of the quantitative physiological parameters extracted through modelling, namely M (a), OEF (b) and CMRO $_2$  (c). OEF and CMRO $_2$  were derived twice, using M obtained from the BH or RS signal modulation experiment (indicated in the figure with the labels 'BH M' and 'RS M'). The maps are reported similarly to Fig. 2. Comparing the group-average maps of BH and RS, the voxel-wise correlations were r=0.58, r=0.28 and r=0.78 for M, OEF and CMRO $_2$ , respectively (all p's<10<sup>-4</sup>).

Fig. 4 reports the scatterplots and the Bland-Altmann plots comparing the average M (a), OEF (b) and CMRO<sub>2</sub> (c) in the GM between BH and RS. Significant associations between the average GM values obtained via the two modulations (BH and RS) were obtained for all parameters (M: r=0.70, OEF: r=0.88, CMRO<sub>2</sub>: r=0.96, all p's<10<sup>-4</sup>). A systematic bias was observed for the different parameters, with an underestimation of RS derived parameters compared to those derived from BH. The M value in the GM was, on average,  $M=7.9\pm2.1$  % for BH and

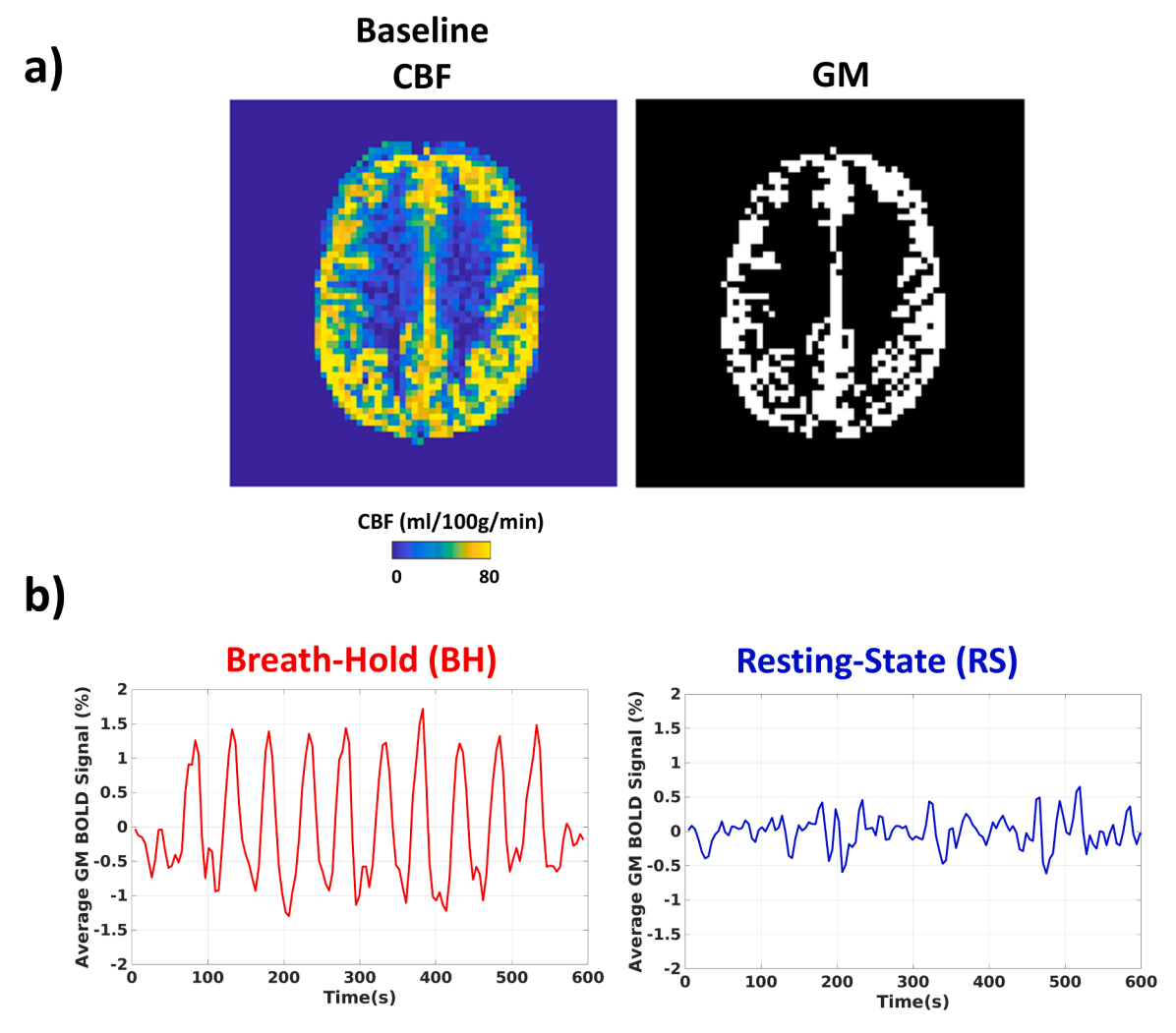


Fig. 1. (a) Example, for a representative subject, of average CBF map and the extracted apparent GM mask. (b) For the same subject as in (a), average GM BOLD signal for the BH and the RS recordings which were then normalized (z-scored) to obtain the global vascular signal to be used as a regressor in the  $CVR_{BOLD}$  and  $CVR_{CBF}$  estimation.

M=6.9±1.8 % for RS with a difference of 12.7% (RS vs. BH: t=-3.59, p<10<sup>-3</sup>). The OEF in the GM was, on average, OEF=36±4 % for BH and OEF=32±6 % for RS with a difference of 11.1% (RS vs. BH: t=-8.1, p<10<sup>-4</sup>). CMRO<sub>2</sub> in the GM was, on average, CMRO<sub>2</sub>=162±35 μmol/100g/min for BH and CMRO<sub>2</sub>=143±33 μmol/100g/min for RS with a difference of 11.7% (RS vs. BH: t=-10.5, p<10<sup>-4</sup>).

Table 1 summarizes the GM values of the main metrics evaluated.

### 3.4. Effect of filtering and recording time on resting-state analysis

Fig. 5 illustrates the impact of band-pass filtering cut-off frequencies and RS recording time on estimating the average M in GM compared to BH. We focus on M as it is the quantitative parameter directly derived from fMRI signals, with brain oxygenation inferred through modeling. The left column displays the average estimation error (bias error), while the right shows the root mean square error (RMSE, combined bias and variance effects). Fig. 5a indicates optimal performance with a low-pass time of 10 s (0.1 Hz). The high-pass cut-off is less critical, with optimal RMSE at around 150 s (0.0067 Hz). These values were used in our analysis. Fig. 5b shows how increased recording time leads to a monotonic reduction in underestimation of average M and RMSE, with average values and confidence intervals presented.

# 4. Discussion

Here, we introduced a novel framework to perform calibrated BOLD-ASL fMRI at rest without a concurrent exogenous modulation in brain physiology. The proposed method is distinguished from other non-invasive MRI methods of mapping  $CMRO_2$  (He et al., 2008; Zhang et al., 2015) by two principal features. Firstly, the method provides a multiparametric mapping of brain physiology, including BOLD-derived and ASL-derived relative vascular reactivities (CVRs). Secondly, the method maps venous oxygenation by exploiting deoxyhemoglobin oscillations over time, delivering an estimate which is virtually unaffected by other sources of magnetic susceptibility.

A fundamental requirement of the method is that the component of the fluctuations of BOLD and ASL signals used to establish the vascular reactivities is of purely vascular origin and unrelated to brain metabolism. We used the global GM BOLD signal as representative of a pure vascular signal based on a previously proposed method applied to standalone BOLD recordings (Liu et al., 2017). Using such a signal, we were able to extract  $CVR_{BOLD}$  and  $CVR_{CBF}$  (in arbitrary units of % signal change) as well as cerebrovascular response latency maps with satisfactory SNR (SNR of the estimate was, on average, around 10 for BOLD and 3.5 for ASL in the GM) and with significant spatial similarities to those extracted with the vasoactive stimulus (hypercapnia induced through breath holding, Fig. 2). Considering that images were not

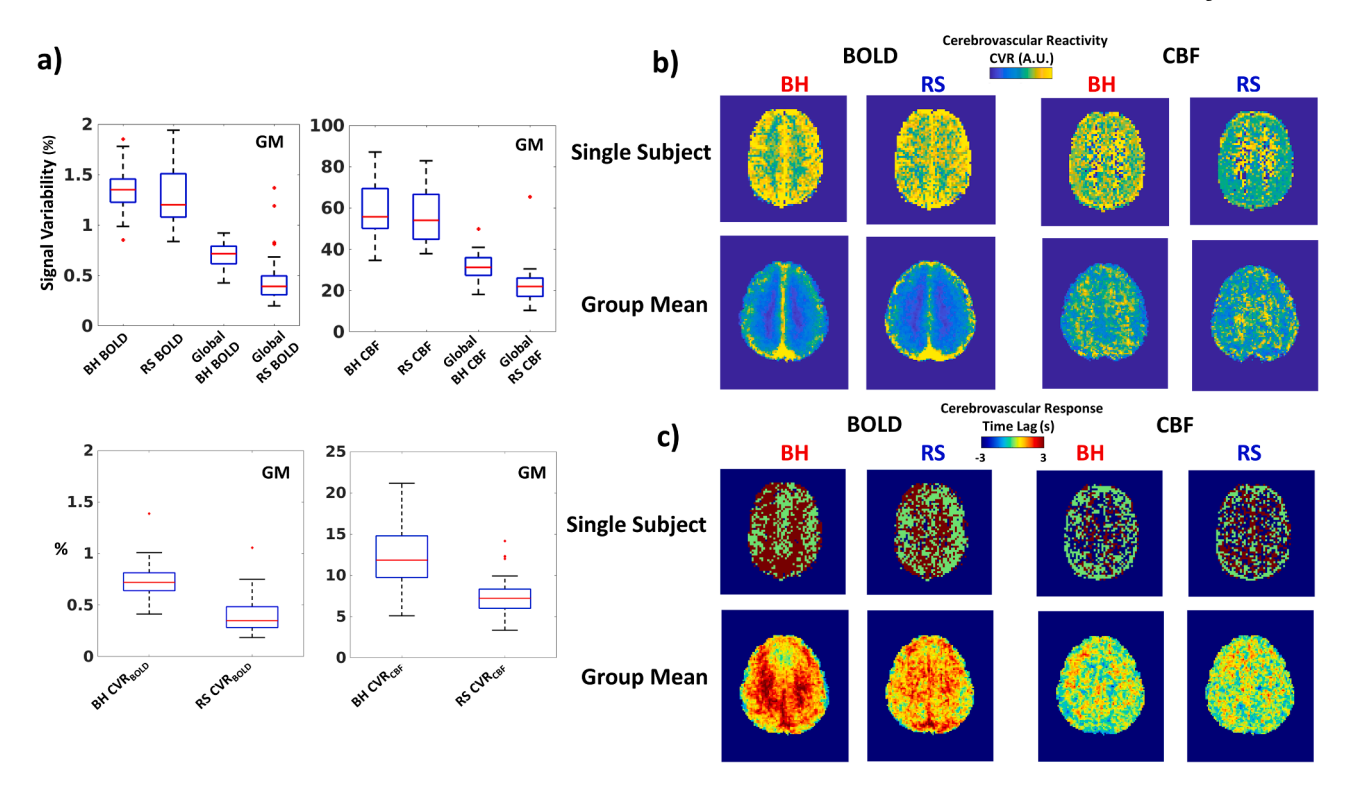
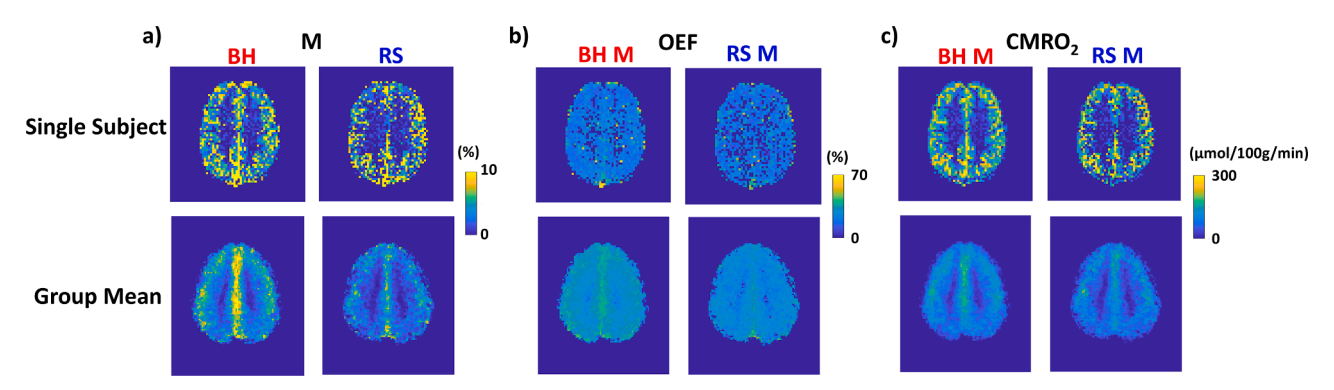


Fig. 2. (a) Boxplots showing the average variability (standard deviation after bandpass filtering) of the voxel-wise and global BOLD (upper row, left image) and CBF (upper row, right image) signals in the GM as well as the CVR<sub>BOLD</sub> and CVR<sub>CBF</sub> (lower row, left image and right image, respectively), during BH and RS. (b,c) Example of parametric maps obtained for a representative subject (upper rows for each subplot) and average maps in MNI space (lower rows for each subplot) related to CVR. The maps are reported when BH (left column for each subplot) or RS (right column for each subplot) was used as experimental paradigm; (b) relative CVR<sub>BOLD</sub> and CVR<sub>CBF</sub> (to highlight the spatial similarities the images were z-scored); (c) CVR<sub>BOLD</sub> and CVR<sub>CBF</sub> response time lags.



**Fig. 3.** Example of parametric maps obtained for a representative subject (upper rows for each subplot) and average maps in MNI space (lower rows for each subplot) for the quantitative physiological parameters extracted from relative CVR<sub>BOLD</sub> and CVR<sub>CBF</sub> through modelling. The maps are reported when BH (left column for each subplot) or RS (right column for each subplot) was used as experimental paradigm. **(a)** M; **(b)** OEF; **(c)** CMRO<sub>2</sub>.

smoothed, and the spatial similarities were evaluated on the entire 3D volume, the correlations obtained for average maps were excellent for  $\rm CVR_{BOLD}$  (r=0.74) and acceptable for  $\rm CVR_{CBF}$  (r=0.23). For the  $\rm CVR_{CBF}$  spatial analysis, it is worth noting that this parameter is characterized by having fewer spatial features compared to  $\rm CVR_{BOLD}$  (which is also weighted by  $\rm CBV_v$ ), contributing to a decrease in the spatial correlations (Biondetti et al., 2024; Zhao et al., 2021). Moreover,  $\rm CVR_{CBF}$  maps are affected by ASL noise in the WM, where the method has a particularly low SNR due to the long arrival times of blood in this compartment). Although expressed in relative units of BOLD or ASL signal change, the resting-state CVR maps did spatially align with the maps derived from breath-holding. This is inherently interesting, as these CVR maps can be utilized to examine local changes in vascular function in patients by spatially comparing brain regions on an individual basis.

With respect to oxygen consumption quantification, the M maps

were similar between RS and BH, with a 3D spatial correlation of the group mean image of r=0.58. Also, the CMRO $_2$  maps were highly similar with a group mean image correlation of r=0.78. For OEF, the spatial correlation was r=0.28. However, the same concept of CVR<sub>CBF</sub> applies to the OEF map, since OEF is known to be largely uniform within the brain in healthy subjects (Fig. 3). Importantly, when evaluating average GM values for M, OEF and CMRO $_2$ , the across-subject associations were high (from r=0.70 to r=0.96, Fig. 4).

The main advantage of the proposed approach of using a global fMRI signal as a regressor to infer CVR and CMRO<sub>2</sub> is that it does not require independent measures, such as a measure of  $P_{\rm ET}{\rm CO}_2$  modulations over time, and it generally provides, especially for BOLD, a signal with good SNR. Please note that  $P_{\rm ET}{\rm CO}_2$  and  $P_{\rm ET}{\rm O}_2$  signals were only used to estimate their average values from which to infer baseline CaCO<sub>2</sub> (and hence  $P_{\rm 50}$ ) and CaO<sub>2</sub>. Temporal averages of end-tidal pressures can be

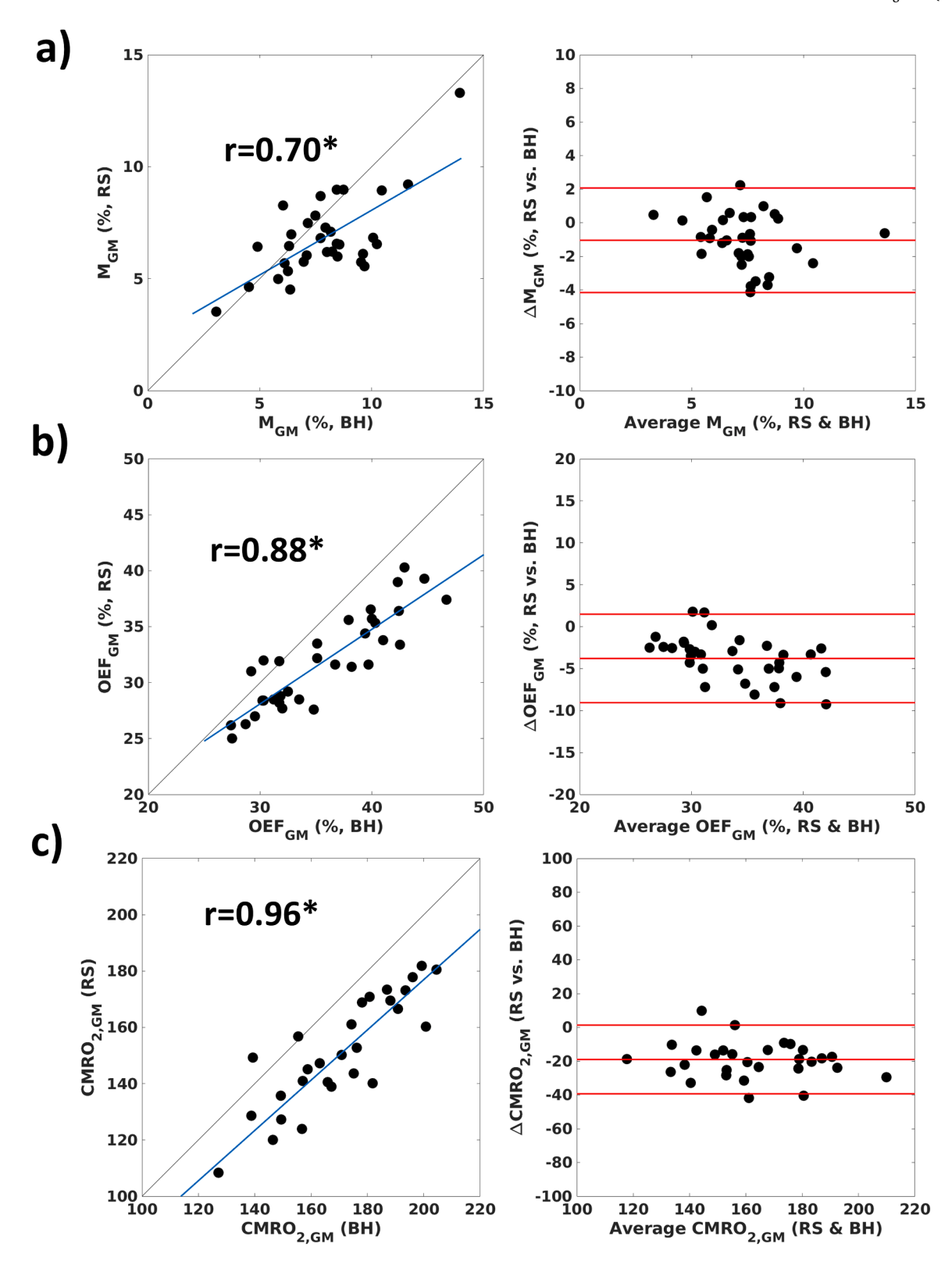


Fig. 4. Scatterplots and the Bland-Altman plots comparing, between BH and RS, global GM (a) M, (b) OEF and (c) CMRO<sub>2</sub>. \* p<10<sup>-4</sup>.

estimated with a much higher accuracy than their small temporal modulations at rest. As a note, we found a variability on baseline  $P_{ET}CO_2$  and  $P_{ET}O_2$  below 10%. Considering an average level of [Hb] of 14 g/dL, this variability should produce a variability of  $P_{50}$  below 4% and a variability of  $CaO_2$ , when the effect of [Hb] is marginalized, below 1%. Although further assessment of the effect of this variability on the modelling parameters estimation is required, when partial pressures of

 $\rm O_2$  and  $\rm CO_2$  in the exhaled air are not available, we suggest using, at least in healthy subjects, standard average values.

When possible, especially in patient populations, these metrics can be assessed through blood sampling. Arterial blood sampling allows for an accurate estimation of  $PaO_2$  and  $PaCO_2$ , which in turn enables the derivation of  $CaO_2$  and  $P_{50}$ . Using end-tidal measurements as a surrogate for arterial gas content has its own limitations, particularly due to the

**Table 1** Average GM values of the main metrics evaluated.  $CVR_{BOLD}$  and  $CVR_{CBF}$  represent the voxel-wise variability of BOLD and CBF signal explained by the normalized global GM BOLD signal (with a 1 TR,  $\pm 4.4$  s, time lag allowed). M, OEF, and  $CMRO_2$  are derived from  $CVR_{BOLD}$  and  $CVR_{CBF}$  through modelling

(Chiarelli et al., 2022a). вн RS Estimated in RS Estimated вн the GM in the GM Voxel-wise CVR<sub>BOLD</sub> 0.74 1.3 1.2 0.40 BOLD  $\pm 0.8\%$  $\pm 0.7\%$ +0.17%+0.18%Signal Variability CVR<sub>CBF</sub> Global BOLD 0.7 0.5  $11.9 \pm 5.1\%$  $7.2 \pm 2.6\%$ Signal  $\pm 0.1\%$  $\pm 0.3\%$ Variability Voxel-wise 58 7.9 + 2.1%6.9+1.8% 59 Maximum CBF Signal +17%+27%BOLD (M) Variability Global CBF 35 25±20 OEF 36±4% 32±6% Signal  $\pm 12\%$ 0/0 Variability CMRO<sub>2</sub> 162 143

 $\pm 35 \mu mol/$ 

100g/min

 $\pm 33 \mu mol$ 

/100g/min

assumption of equilibrium between arterial and alveolar gas pressures (Bengtsson et al., 2001). Additionally, the current study employed a nasal cannula to monitor  $O_2$  and  $CO_2$  in the expired air, which requires participants to breathe almost exclusively through their nose (Bright and Murphy, 2013). A pulse oximeter may also be used to derive  $CaO_2$ , when coupled at least with measures of hematocrit. Indeed, arterial or venous blood sampling can allow for an accurate estimation of hematocrit, which in this study was inferred using quantitative measures of the venous T1 relaxation in the superior sagittal sinus. Although the MRI method has been proven to be accurate (Varela et al., 2011), more direct measurements of hematocrit in blood are preferrable in future studies, particularly for clinical applications where a large variability in hemoglobin in blood may be found.

Importantly, the use of a global signal regressor was already validated by our group for the BH task (Driver et al., 2024). When applying the approach to BH, the method inherently accounts for several confounding factors introduced by the hypercapnic BH stimulus (Thomason et al., 2005). The BH outcome depends on patient compliance and factors such as expiration time, lung volume, arterial transit time from the lung and brain hemodynamics time constant. These factors are largely accounted for by using a global brain signal as a regressor. The main remaining confounding factor when using BH and a global regressor is movement. However, we demonstrated in our previous work that movement does not seem to heavily affect the results when simple movement correction algorithms are implemented (Driver et al., 2024).

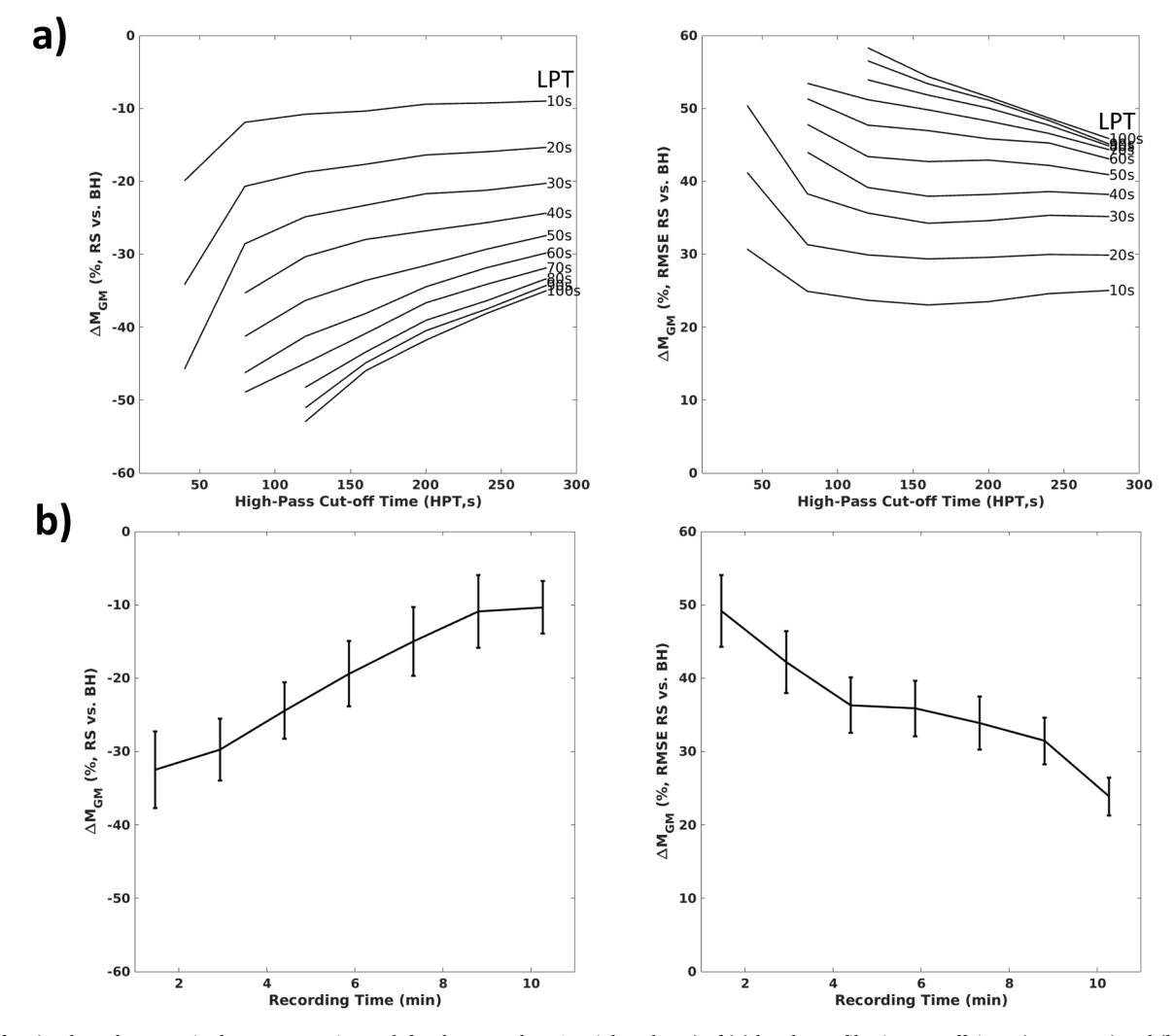


Fig. 5. Effect (evaluated as error in the average estimate, left column, and RMSE, right column) of (a) band-pass filtering cut-off times (upper row) and (b) recording time (lower row) on RS estimation of GM M compared to the estimation performed through BH. Confidence intervals of the means are reported in (b) but not in (a).

The drawback of using a global brain signal as a regressor is the absence of CVR quantification. However, since the maximum BOLD modulation is derived from the comparison of  $\text{CVR}_{\text{BOLD}}$  and  $\text{CVR}_{\text{CBF}}$  (i.e., approximately their ratio), quantification is not required for our application; only the use of the same regressor to estimate both CVRs is necessary.

We considered using a global CBF signal from our concurrent ASL data as a vascular regressor instead of the BOLD signal. However, this approach underperformed, likely due to ASL's lower SNR compared to BOLD, leading to an underestimation of M for RS. Using the GM global BOLD signal as a regressor still showed a residual negative bias of about 10 % in M estimation using RS compared to BH, affecting OEF and CMRO2 estimates (Fig. 4). This bias was partially due to limited recording time. Increasing the recording time reduced the bias error in RS-M compared to BH-M, as shown by a monotonic decrease without a plateau within our 10-minute limit (Fig. 5b). The RMSE plot confirmed that the maximum recording time was insufficient to minimize error. We speculate that the decreasing bias with longer recording times stems from spurious correlations between global vascular signals and local brain metabolism, which are stronger with limited data samples. The resting-state method requires longer acquisition times beyond 10 minutes, likely due to the limited temporal SNR of ASL and smaller endogenous vascular modulations compared to exogenous stimuli.

Nonetheless, it is well known that resting-state signals, both at a regional and global level, are generated by a mixture of physiological and non-physiological effects, which are very complex to discriminate. Some of these effects, such as head motion or neural activity, are unwanted for our application (Ciric et al., 2018; Power et al., 2017; Schölvinck et al., 2010). In an approach aimed at minimizing these unwanted contributions, we decided to implement a data-driven approach for frequency selection of the resting-state signals of interest. An analysis of filtering effects identified the high-frequency spectrum (oscillation time below 20 s, frequency above 0.05 Hz) as crucial for the approach. With a TR of 4.4 s and the need to remove perfusion signal weighting from tag-control alternation, we theoretically could explore a minimum oscillation time of 8.8 s, that we approximated with a low-pass cut-off time of at least 10 s (0.1 Hz). Filtering out frequencies with oscillation times between 10 s and 20 s (0.05 Hz to 0.1 Hz) nearly doubled the bias error (from -10 % to -20 %) and significantly increased the RMSE (Fig. 5a). This suggests that vascular modulations from respiration and fast systemic pressure changes are key for estimating M, though not the only contributors, as the optimal high-pass time was around 150 s (0.0067 Hz, lowest RMSE).

In summary, we found that, with long resting-state (RS) acquisitions and optimized image and signal processing, the associations between the parameters of interest estimated at RS and during BH were good. This result suggests that the band-pass filtered global BOLD signal within the gray matter (GM) can be a good proxy for a vasodilatory signal, unrelated to local brain activity. However, other physiological effects cannot be completely ruled out. The lower estimate of M during RS compared to BH (RS estimate of M about 10 % lower than BH) maybe attributable to local CMRO2 increases synchronous with the global GM BOLD signal during RS, or conversely, to an absence of isometabolism during BH, resulting in decreased brain activity and CMRO2 during hypercapnia. Regarding the latter, some studies have shown that hypercapnia tends to reduce neural activity and CMRO<sub>2</sub> (the two are tightly linked in humans) with a maximum CMRO2 decrease reported of up to 20 % (Baas et al., 2023; Deckers et al., 2022; James et al., 2023; Zappe et al., 2008). This modulation would reflect an increase in the BOLD signal with respect to flow between 5 % and 10 %, which is compatible with the bias we identified in M between RS and BH. However, further studies where longer RS recordings are acquired together with a BH task, or another vasodilatory stimulation, and with alternative MRI and non-MRI approaches that map CMRO2, are required to establish the maximum accuracy achievable by the RS method and the underlying methodological or physiological origin of any residual errors.

The method shares limitations with other calibrated fMRI

approaches. It combines BOLD with ASL functional measures, with ASL having a low temporal SNR and being limited mostly to estimate perfusion in GM. Additionally, with the relatively short post-labelling delays used for functional assessment (PLD=1.5 s), the ASL measures may be inaccurate in the elderly or patients population where there may be a longer arterial transit times from the blood tagging region to the tissue. Moreover, the method requires a vascular reserve, which may be absent in diseases with compromised vasculature, such as ischemic stroke, where arteries may be fully dilated. We have shown that estimating baseline oxygen metabolism from a single hypercapnic fMRI calibration is reliable unless mean transit time through microvasculature and mitochondrial oxygen tension are both high (MCTT over 2-3 seconds and PmO2 over 20-30 mmHg) (Chiarelli et al., 2022a). This can occur in cases of severe physiological and metabolic dysfunction. For example, a significant rise in PmO<sub>2</sub> may occur when the oxygen delivered by arterial blood remains high, even though the tissue is not consuming it due to mitochondrial dysfunction or brain tissue necrosis.

The method allows for calibrated fMRI with a simple resting paradigm, enabling the estimation of critical brain physiology parameters that may reflect pathology, supporting its potential for routine use in neuroscience and clinical imaging.

#### Data availability statement

Raw data in BIDS format is openly accessible from: https://git.cardiff .ac.uk/cubric/wand

 ${\bf Code\ is\ available\ at:\ https://github.com/chiarell/Hypercapnic-Cal\ ibrated-fMRI}$ 

#### CRediT authorship contribution statement

Antonio M. Chiarelli: Writing – review & editing, Writing – original draft, Visualization, Validation, Supervision, Project administration, Methodology, Investigation, Funding acquisition, Formal analysis, Conceptualization. Michael Germuska: Supervision, Methodology, Funding acquisition, Data curation, Conceptualization. Davide Di Censo: Writing - review & editing, Methodology, Formal analysis. Ian Driver: Writing - review & editing, Investigation. Maria Eugenia Caligiuri: Writing - review & editing, Supervision, Resources, Funding acquisition. Hannah Thomas: Writing - review & editing, Investigation. Svetla Manolova: Writing - review & editing, Investigation. Hannah L Chandler: Writing - review & editing, Investigation. Alessandra Caporale: Writing – review & editing, Visualization, Validation, Methodology. Emma Biondetti: Writing - review & editing, Writing original draft, Visualization, Validation, Funding acquisition. Richard G. Wise: Writing - review & editing, Writing - original draft, Visualization, Validation, Supervision, Resources, Project administration, Funding acquisition.

#### **Declaration of competing interest**

The authors declare no competing financial and non-financial interests.

#### Acknowledgments

Funded by:

EU-NextGenEU- Italian MUR, PNR and PRIN, n. 2022BERM2F, "Mapping Mitochondrial Function and Oxygen Metabolism in the Human Brain with Magnetic Resonance Imaging."

EU-NextGenEU- Italian MUR, PNRR and PRIN, n. P20225AEEE, "Hybrid PET-MRI to simultaneously probe brain metabolism and cerebrovascular function in neurodegenerative diseases."

EU-NextGenEU- Italian MUR, PNRR and PRIN, n. P2022ESHT4, "Advancing MRI biomarkers of brain tissue microstructure and energetics in Multiple Sclerosis."

EU-NextGenEU, Italian MUR, PNRR, n. ECS00000041, "VITALITY - Innovation, digitalization and sustainability for the diffused economy in Central Italy."

EU-NextGenEU, Italian MUR, PNRR, n. PE00000006, "MNESYS—A Multiscale integrated approach to the study of the nervous system in health and disease."

EU-NextGenEU- Italian MUR, PNR and PRIN, n. 2022MHMSSJ, "Combining magnetic resonance imaging and optical spectroscopy to map microvascular function and oxygen metabolism in healthy and diseased brain."

Data were acquired as part of the Welsh Advanced Neuroimaging Database, which was funded by a Wellcome Trust Strategic Award [104943/Z/14/Z]

EB has received funding from the European Union's Horizon Europe research and innovation programme under the Marie Skłodowska-Curie Grant Agreement No. 101066055—acronym HERMES.

MG is supported by the Wellcome Trust [220575/Z/20/Z] and received support from the Engineering and Physical Sciences Research Council [EP/S025901/1].

#### Data availability

Data availability statement: Raw data in BIDS format is openly accessible from: https://git.cardiff.ac.uk/cubric/wand.

#### References

- Alsop, D.C., Detre, J.A., Golay, X., Günther, M., Hendrikse, J., Hernandez-Garcia, L., Lu, H., MacIntosh, B.J., Parkes, L.M., Smits, M., Osch, M.J.P.van, Wang, D.J.J., Wong, E.C., Zaharchuk, G., 2015. Recommended implementation of arterial spinlabeled perfusion MRI for clinical applications: a consensus of the ISMRM perfusion study group and the European consortium for ASL in dementia. Magn. Reson. Med. 73, 102–116. https://doi.org/10.1002/mrm.25197.
- Aslan, S., Xu, F., Wang, P.L., Uh, J., Yezhuvath, U.S., van Osch, M., Lu, H., 2010. Estimation of labeling efficiency in pseudocontinuous arterial spin labeling. Magn. Reson. Med. 63, 765–771. https://doi.org/10.1002/mrm.22245.
- Avants, B.B., Tustison, N.J., Song, G., Cook, P.A., Klein, A., Gee, J.C., 2011.
  A reproducible evaluation of ANTs similarity metric performance in brain image registration. NeuroImage 54, 2033–2044. https://doi.org/10.1016/j.neuroimage.2010.09.025.
- Baas, K.P.A., Vu, C., Shen, J., Coolen, B.F., Biemond, B.J., Strijkers, G.J., Wood, J.C., Nederveen, A.J., 2023. Venous blood oxygenation measurements using TRUST and T2-TRIR MRI during hypoxic and hypercapnic gas challenges. J. Magn. Reson. Imaging 58, 1903–1914. https://doi.org/10.1002/jmri.28744.
- Bengtsson, J., Bake, B., Johansson, Å., Bengtson, J.P., 2001. End-tidal to arterial oxygen tension difference as an oxygenation index. Acta Anaesthesiol. Scand. 45, 357–363. https://doi.org/10.1034/j.1399-6576.2001.045003357.x.
- Biondetti, E., Chiarelli, A.M., Germuska, M., Lipp, I., Villani, A., Caporale, A.S., Patitucci, E., Murphy, K., Tomassini, V., Wise, R.G., 2024. Breath-hold BOLD fMRI without CO2 sampling enables estimation of venous cerebral blood volume: potential use in normalization of stimulus-evoked BOLD fMRI data. NeuroImage 285, 120492. https://doi.org/10.1016/j.neuroimage.2023.120492.
- Birn, R.M., Smith, M.A., Jones, T.B., Bandettini, P.A., 2008. The respiration response function: The temporal dynamics of fMRI signal fluctuations related to changes in respiration. NeuroImage 40, 644–654. https://doi.org/10.1016/j. neuroimage.2007.11.059.
- Biswal, B.B., Kannurpatti, S.S., Rypma, B., 2007. Hemodynamic scaling of fMRI-BOLD signal: validation of low frequency spectral amplitude as a scalability factor. Magn. Reson. Imaging 25, 1358–1369. https://doi.org/10.1016/j.mri.2007.03.022.
- Bright, M.G., Croal, P.L., Blockley, N.P., Bulte, D.P., 2019. Multiparametric measurement of cerebral physiology using calibrated fMRI. NeuroImage 187, 128–144. https:// doi.org/10.1016/j.neuroimage.2017.12.049.
- Bright, M.G., Murphy, K., 2013. Reliable quantification of BOLD fMRI cerebrovascular reactivity despite poor breath-hold performance. NeuroImage 83, 559–568. https://doi.org/10.1016/j.neuroimage.2013.07.007.
- Bulte, D.P., Kelly, M., Germuska, M., Xie, J., Chappell, M.A., Okell, T.W., Bright, M.G., Jezzard, P., 2012. Quantitative measurement of cerebral physiology using respiratory-calibrated MRI. NeuroImage 60, 582–591. https://doi.org/10.1016/j. neuroImage.2011.12.017.
- Buxton, R.B., 2009. Introduction to Functional Magnetic Resonance Imaging: Principles and Techniques. Cambridge University Press.
- Carrera, E., Lee, L.K., Giannopoulos, S., Marshall, R.S., 2009. Cerebrovascular reactivity and cerebral autoregulation in normal subjects. J. Neurol. Sci. 285, 191–194. https://doi.org/10.1016/j.jns.2009.06.041.
- Chandler, H.L., Stickland, R.C., Patitucci, E., Germuska, M., Chiarelli, A.M., Foster, C., Bhome-Dhaliwal, S., Lancaster, T.M., Saxena, N., Khot, S., Tomassini, V., Wise, R.G., 2023. Reduced brain oxygen metabolism in patients with multiple sclerosis: evidence from dual-calibrated functional MRI. J. Cereb. Blood Flow Metab. Off. J.

- Int. Soc. Cereb. Blood Flow Metab. 43, 115–128. https://doi.org/10.1177/0271678x221121849.
- Chang, C., Glover, G.H., 2009. Relationship between respiration, end-tidal CO2, and BOLD signals in resting-state fMRI. NeuroImage 47, 1381–1393. https://doi.org/ 10.1016/j.neuroimage.2009.04.048.
- Chen, J.J., Uthayakumar, B., Hyder, F., 2022. Mapping oxidative metabolism in the human brain with calibrated fMRI in health and disease. J. Cereb. Blood Flow Metab. 42, 1139–1162. https://doi.org/10.1177/0271678x221077338.
- Chiarelli, Antonio M, Germuska, M., Chandler, H., Stickland, R., Patitucci, E., Biondetti, E., Mascali, D., Saxena, N., Khot, S., Steventon, J., Foster, C., Rodríguez-Soto, A.E., Englund, E., Murphy, K., Tomassini, V., Wehrli, F.W., Wise, R.G., 2022a. A flow-diffusion model of oxygen transport for quantitative mapping of cerebal metabolic rate of oxygen (CMRO2) with single gas calibrated fMRI. J. Cereb. Blood Flow Metab. 42, 1192–1209. https://doi.org/10.1177/0271678x221077332.
- Chiarelli, Antonio Maria, Villani, A., Mascali, D., Petsas, N., Biondetti, E., Caporale, A., Digiovanni, A., Grasso, E.A., Ajdinaj, P., D'Apolito, M., Rispoli, M.G., Sensi, S., Murphy, K., Pozzilli, C., Wise, R.G., Tomassini, V., 2022b. Cerebrovascular reactivity in multiple sclerosis is restored with reduced inflammation during immunomodulation. Sci. Rep. 12, 15453. https://doi.org/10.1038/s41598-022-19113-8
- Ciric, R., Rosen, A.F.G., Erus, G., Cieslak, M., Adebimpe, A., Cook, P.A., Bassett, D.S., Davatzikos, C., Wolf, D.H., Satterthwaite, T.D., 2018. Mitigating head motion artifact in functional connectivity MRI. Nat. Protoc. 13, 2801–2826. https://doi.org/ 10.1038/s41596-018-0065-y.
- Davis, T.L., Kwong, K.K., Weisskoff, R.M., Rosen, B.R., 1998. Calibrated functional MRI: mapping the dynamics of oxidative metabolism. Proc. Natl. Acad. Sci. 95, 1834–1839. https://doi.org/10.1073/pnas.95.4.1834.
- Deckers, P.T., Bhogal, A.A., Dijsselhof, M.B., Faraco, C.C., Liu, P., Lu, H., Donahue, M.J., Siero, J.C., 2022. Hemodynamic and metabolic changes during hypercapnia with normoxia and hyperoxia using pCASL and TRUST MRI in healthy adults. J. Cereb. Blood Flow Metab. 42, 861–875. https://doi.org/10.1177/0271678x211064572.
- Driver, I.D., Chiarelli, A.M., Chandler, H.L., Thomas, H., Manolova, S., Lu, H., Wise, R.G., Germuska, M., 2024. Breath-hold calibrated fMRI mapping of absolute cerebral metabolic rate of oxygen metabolism (CMRO2): an assessment of the accuracy and repeatability in a healthy adult population. Imaging Neurosci. 2, 1–14. https://doi. org/10.1162/imag a 00298.
- Friston, K.J., 1994. Statistical parametric mapping. Functional Neuroimaging: Technical Foundations. Academic Press, San Diego, CA, US, pp. 79–93.
- Fukunaga, M., Horovitz, S.G., de Zwart, J.A., van Gelderen, P., Balkin, T.J., Braun, A.R., Duyn, J.H., 2008. Metabolic origin of bold signal fluctuations in the absence of stimuli. J. Cereb. Blood Flow Metab. 28, 1377–1387. https://doi.org/10.1038/ icbfm.2008.25.
- Gai, X., Taki, K., Kato, H., Nagaishi, H., 2003. Regulation of hemoglobin affinity for oxygen by carbonic anhydrase. J. Lab. Clin. Med. 142, 414–420. https://doi.org/ 10.1016/j.lab.2003.07.001.
- Gauthier, C.J., Desjardins-Crépeau, L., Madjar, C., Bherer, L., Hoge, R.D., 2012. Absolute quantification of resting oxygen metabolism and metabolic reactivity during functional activation using QUO2 MRI. NeuroImage 63, 1353–1363. https://doi. org/10.1016/j.neuroimage.2012.07.065.
- Gauthier, C.J., Hoge, R.D., 2012. Magnetic resonance imaging of resting OEF and CMRO<sub>2</sub> using a generalized calibration model for hypercapnia and hyperoxia. NeuroImage 60, 1212–1225. https://doi.org/10.1016/j.neuroimage.2011.12.056.
- Germuska, M., Chandler, H.L., Stickland, R.C., Foster, C., Fasano, F., Okell, T.W., Steventon, J., Tomassini, V., Murphy, K., Wise, R.G., 2019. Dual-calibrated fMRI measurement of absolute cerebral metabolic rate of oxygen consumption and effective oxygen diffusivity. NeuroImage 184, 717–728. https://doi.org/10.1016/j. neuroimage.2018.09.035.
- Germuska, M., Wise, R.G., 2019. Calibrated fMRI for mapping absolute CMRO2: practicalities and prospects. NeuroImage, Physiol. Quant. MRI 187, 145–153. https://doi.org/10.1016/j.neuroimage.2018.03.068.
- Gjedde, A., 2002. Cerebral blood flow change in arterial hypoxemia is consistent with negligible oxygen tension in brain mitochondria. NeuroImage 17, 1876–1881. https://doi.org/10.1006/nimg.2002.1272.
- Gjedde, A., Poulsen, P.H., Østergaard, L., 1999. On the oxygenation of hemoglobin in the Human brain. In: Eke, A., Delpy, D.T. (Eds.), Oxygen Transport to Tissue XXI, Advances in Experimental Medicine and Biology. Springer US, Boston, MA, pp. 67–81. https://doi.org/10.1007/978-1-4615-4717-4\_9.
- Golestani, A.M., Wei, L.L., Chen, J.J., 2016. Quantitative mapping of cerebrovascular reactivity using resting-state BOLD fMRI: validation in healthy adults. NeuroImage 138, 147–163. https://doi.org/10.1016/j.neuroimage.2016.05.025.
- Grubb, R.L., Raichle, M.E., Eichling, J.O., Ter-Pogossian, M.M., 1974. The effects of changes in PaCO2 cerebral blood volume. Blood Flow, and Vascular Mean Transit Time. Stroke 5, 630–639. https://doi.org/10.1161/01.STR.5.5.630.
- Hayashi, T., Watabe, H., Kudomi, N., Kim, K.M., Enmi, J.-I., Hayashida, K., Iida, H., 2003. A theoretical model of oxygen delivery and metabolism for physiologic interpretation of quantitative cerebral blood flow and metabolic rate of oxygen. J. Cereb. Blood Flow Metab. Off. J. Int. Soc. Cereb. Blood Flow Metab. 23, 1314–1323. https://doi.org/10.1097/01.WCB.0000090506.76664.00.
- He, X., Zhu, M., Yablonskiy, D.A., 2008. Validation of oxygen extraction fraction measurement by qBOLD technique. Magn. Reson. Med. 60, 882–888. https://doi. org/10.1002/mrm.21719
- Hoge, R.D., 2012. Calibrated fMRI. NeuroImage, 20 years of fMRI 62, 930–937. https://doi.org/10.1016/j.neuroimage.2012.02.022.
- Hyder, F., Shulman, R.G., Rothman, D.L., 1998. A model for the regulation of cerebral oxygen delivery. J. Appl. Physiol. 85, 554–564. https://doi.org/10.1152/ jappl.1998.85.2.554.

Insiripong, S., Supattarobol, T., Jetsrisuparb, A., 2013. Comparison of hematocrit/ hemoglobin ratios in subjects with alpha-thalassemia, with subjects having chronic kidney disease and normal subjects. Southeast Asian J. Trop. Med. Public Health 44, 707–711

A.M. Chiarelli et al.

- James, S., Sanggaard, S., Akif, A., Mishra, S.K., Sanganahalli, B.G., Blumenfeld, H., Verhagen, J.V., Hyder, F., Herman, P., 2023. Spatiotemporal features of neurovascular (un)coupling with stimulus-induced activity and hypercapnia challenge in cerebral cortex and olfactory bulb. J. Cereb. Blood Flow Metab. 43, 1891–1904. https://doi.org/10.1177/0271678x231183887.
- Jenkinson, M., Bannister, P., Brady, M., Smith, S., 2002. Improved optimization for the robust and accurate linear registration and motion correction of brain images. NeuroImage 17, 825–841. https://doi.org/10.1016/s1053-8119(02)91132-8.
- Jenkinson, M., Beckmann, C.F., Behrens, T.E.J., Woolrich, M.W., Smith, S.M., 2012. FSL. NeuroImage, 20 years of fMRI 62, 782–790. https://doi.org/10.1016/j.neuroimage. 2011.09.015.
- Kannurpatti, S.S., Biswal, B.B., 2008. Detection and scaling of task-induced fMRI-BOLD response using resting state fluctuations. NeuroImage 40, 1567–1574. https://doi.org/10.1016/j.neuroimage.2007.09.040.
- Kannurpatti, S.S., Motes, M.A., Rypma, B., Biswal, B.B., 2011. Increasing measurement accuracy of age-related BOLD signal change: minimizing vascular contributions by resting-state-fluctuation-of-amplitude scaling. Hum. Brain Mapp. 32, 1125–1140. https://doi.org/10.1002/bbm.21097.
- Kida, I., Kennan, R.P., Rothman, D.L., Behar, K.L., Hyder, F., 2000. High-resolution CMR (O2) mapping in rat cortex: a multiparametric approach to calibration of BOLD image contrast at 7 tesla. J. Cereb. Blood Flow Metab. Off. J. Int. Soc. Cereb. Blood Flow Metab. 20, 847–860. https://doi.org/10.1097/00004647-200005000-00012.
- Liu, P., De Vis, J.B., Lu, H., 2019. Cerebrovascular reactivity (CVR) MRI with CO2 challenge: a technical review. NeuroImage, Physiol. Quant. MRI 187, 104–115. https://doi.org/10.1016/j.neuroImage.2018.03.047.
- Liu, P., Li, Y., Pinho, M., Park, D.C., Welch, B.G., Lu, H., 2017. Cerebrovascular reactivity mapping without gas challenges. NeuroImage 146, 320–326. https://doi.org/ 10.1016/j.neuroimage.2016.11.054.
- Lu, H., Clingman, C., Golay, X., van Zijl, P.C.M., 2004. Determining the longitudinal relaxation time (T1) of blood at 3.0 tesla. Magn. Reson. Med. 52, 679–682. https://doi.org/10.1002/mrm.20178.
- Macey, P.M., Macey, K.E., Kumar, R., Harper, R.M., 2004. A method for removal of global effects from fMRI time series. NeuroImage 22, 360–366. https://doi.org/ 10.1016/j.neuroimage.2003.12.042.
- Magistretti, P., Allaman, I., 2013. Brain energy metabolism. Neurosci. 21st Century Basic Clin. 1591–1620. https://doi.org/10.1007/978-1-4614-1997-6-56.
- Murphy, K., Birn, R.M., Bandettini, P.A., 2013. Resting-state fMRI confounds and cleanup. NeuroImage, Mapp. Connectome 80, 349–359. https://doi.org/10.1016/j. neuroImage.2013.04.001.
- Murphy, K., Birn, R.M., Handwerker, D.A., Jones, T.B., Bandettini, P.A., 2009. The impact of global signal regression on resting state correlations: are anti-correlated networks introduced? NeuroImage 44, 893–905. https://doi.org/10.1016/j. neuroimage.2008.09.036.
- Mutsaerts, H.J.M.M., Steketee, R.M.E., Heijtel, D.F.R., Kuijer, J.P.A., Osch, M.J.P.van, Majoie, C.B.L.M., Smits, M., Nederveen, A.J., 2014. Inter-vendor reproducibility of pseudo-continuous arterial spin labeling at 3 tesla. PLOS ONE 9, e104108. https://doi.org/10.1371/journal.pone.0104108.
- Okell, T.W., Chappell, M.A., Kelly, M.E., Jezzard, P., 2013. Cerebral blood flow quantification using vessel-encoded arterial spin labeling. J. Cereb. Blood Flow Metab. 33, 1716–1724. https://doi.org/10.1038/jcbfm.2013.129.
- Pillai, J.J., Mikulis, D.J., 2015. Cerebrovascular reactivity mapping: an evolving standard for clinical Functional imaging. Am. J. Neuroradiol. 36, 7–13. https://doi.org/ 10.3174/ajnr.A3941.

- Power, J.D., Plitt, M., Laumann, T.O., Martin, A., 2017. Sources and implications of whole-brain fMRI signals in humans. NeuroImage 146, 609–625. https://doi.org/ 10.1016/j.neuroimage.2016.09.038.
- Raz, N., Rodrigue, K.M., Kennedy, K.M., Acker, J.D., 2007. Vascular health and longitudinal changes in brain and cognition in middle-aged and older adults. Neuropsychology 21, 149–157. https://doi.org/10.1037/0894-4105.21.2.149.
- Rogers, B.P., Morgan, V.L., Newton, A.T., Gore, J.C., 2007. Assessing functional connectivity in the human brain by fMRI. Magn. Reson. Imaging 25, 1347–1357. https://doi.org/10.1016/j.mri.2007.03.007.
- Schmithorst, V.J., Hernandez-Garcia, L., Vannest, J., Rajagopal, A., Lee, G., Holland, S. K., 2014. Optimized simultaneous ASL and BOLD functional imaging of the whole brain. J. Magn. Reson. Imaging JMRI 39, 1104–1117. https://doi.org/10.1002/imri\_24273
- Schölvinck, M.L., Maier, A., Ye, F.Q., Duyn, J.H., Leopold, D.A., 2010. Neural basis of global resting-state fMRI activity. Proc. Natl. Acad. Sci. 107, 10238–10243. https://doi.org/10.1073/pnas.0913110107.
- Smith, S.M., Jenkinson, M., Woolrich, M.W., Beckmann, C.F., Behrens, T.E.J., Johansen-Berg, H., Bannister, P.R., De Luca, M., Drobnjak, I., Flitney, D.E., Niazy, R.K., Saunders, J., Vickers, J., Zhang, Y., De Stefano, N., Brady, J.M., Matthews, P.M., 2004. Advances in functional and structural MR image analysis and implementation as FSL. NeuroImage 23 (Suppl 1), S208–S219. https://doi.org/10.1016/j.neuroimage.2004.07.051.
- Tak, S., Polimeni, J.R., Wang, D.J.J., Yan, L., Chen, J.J., 2015. Associations of resting-State fMRI functional connectivity with flow-BOLD coupling and regional vasculature. Brain Connect 5, 137–146. https://doi.org/10.1089/brain.2014.0299.
- Thomason, M.E., Burrows, B.E., Gabrieli, J.D.E., Glover, G.H., 2005. Breath holding reveals differences in fMRI BOLD signal in children and adults. NeuroImage 25, 824–837. https://doi.org/10.1016/j.neuroimage.2004.12.026.
- Thomason, M.E., Foland, L.C., Glover, G.H., 2006. Calibration of BOLD fMRI using breath holding reduces group variance during a cognitive task. Hum. Brain Mapp. 28, 59–68. https://doi.org/10.1002/hbm.20241.
- Varela, M., Hajnal, J.V., Petersen, E.T., Golay, X., Merchant, N., Larkman, D.J., 2011.
  A method for rapid in vivo measurement of blood T1. NMR Biomed 24, 80–88.
  <a href="https://doi.org/10.1002/nbm.1559">https://doi.org/10.1002/nbm.1559</a>.
- Watts, M.E., Pocock, R., Claudianos, C., 2018. Brain energy and oxygen metabolism: emerging role in normal function and disease. Front. Mol. Neurosci. 11.
- Wise, R.G., Ide, K., Poulin, M.J., Tracey, I., 2004. Resting fluctuations in arterial carbon dioxide induce significant low frequency variations in BOLD signal. NeuroImage 21.
- Zappe, A.C., Uludağ, K., Oeltermann, A., Uğurbil, K., Logothetis, N.K., 2008. The influence of moderate hypercapnia on neural activity in the anesthetized nonhuman primate. Cereb. Cortex 18, 2666–2673. https://doi.org/10.1093/cercor/bhn023.
- Zauner, A., Daugherty, W.P., Bullock, M.R., Warner, D.S., 2002. Brain Oxygenation and energy metabolism: part I—biological function and pathophysiology. Neurosurgery 51, 289
- Zhang, J., Liu, T., Gupta, A., Spincemaille, P., Nguyen, T.D., Wang, Y., 2015.
  Quantitative mapping of cerebral metabolic rate of oxygen (CMRO2) using quantitative susceptibility mapping (QSM). Magn. Reson. Med. 74, 945–952.
  https://doi.org/10.1002/mrm.25463
- Zhao, M.Y., Fan, A.P., Chen, D.Y.-T., Sokolska, M.J., Guo, J., Ishii, Y., Shin, D.D., Khalighi, M.M., Holley, D., Halbert, K., Otte, A., Williams, B., Rostami, T., Park, J.-H., Shen, B., Zaharchuk, G., 2021. Cerebrovascular reactivity measurements using simultaneous 15O-water PET and ASL MRI: impacts of arterial transit time, labeling efficiency, and hematocrit. NeuroImage 233, 117955. https://doi.org/10.1016/j.neuroImage.2021.117955.